Geometry Optimization of DC and SRF Guns to Maximize Beam Brightness

M.N. Lakshmanan and I.V. Bazarov, CLASSE, Cornell University, Ithaca, NY 14853, USA
T. Miyajima, Photon Factory, KEK, Tsukuba, Japan

Abstract

A set of geometries for DC and SRF guns is studied from the perspective of beam dynamics. The geometries are parameterized and are made a part of an optimization process that minimizes emittance downstream of the gun following the emittance compensation solenoid. The setups simulated are kept to realistic field strengths by imposing an empirical gun voltage breakdown law in the DC gun case and a maximum achievable surface magnetic field for the SRF gun case.

INTRODUCTION

To realize their fullest potential for a range of applications, Energy Recovery Linacs require high brightness high current electron sources operating beyond the state of the art. Photoemission guns, operating with either DC or continuous duty RF fields, are the technology of choice. Very high accelerating gradients at the photocathodes are required to counteract the space charge forces acting on the electron bunches. In DC guns, the strength of the field is typically limited by the field emission and related high voltage breakdown phenomena. Superconducting RF (SRF) guns have the potential to overcome the limitations imposed on DC guns and allow higher operating gradients. The highest accelerating field that can be supported in an SRF gun is limited by the highest (critical) magnetic field on the cavity surface which leads to cavity quenching, even though other practical causes (e.g. field emission) may limit the gradient to much lower values. To transport the space charge dominated beam from the gun to an energy boosting linac, a high gun voltage is also desirable. In addition to high longitudinal accelerating field, field components leading to transverse focusing in the gun are important to ensure proper beam matching and high degree of emittance compensation.

Overall, the gun design is subject to a number of conflicting requirements. For a example, a stronger transverse focusing in DC guns via cathode electrode shaping typically reduces the available accelerating field otherwise possible for the same cathode-anode separation and gun voltage. Similarly, empirical data on voltage breakdown for large area in-vacuum electrodes suggests that much higher gradients are possible at the expense of a shorter gap between the electrodes and the correspondingly reduced gun voltage. Time-varying nature of fields in SRF guns introduces additional complications: the optimal phase of laser pulse arrival can be chosen either to maximize the accelerating gradient at the photocathode, the beam energy at the exit of the gun, or by requiring that the transverse momentum imparted to off-axis particles in the gun nearly does not depend on the position of particles inside the bunch [1]. All these considerations in turn are a function of the gun geometry making it a critical factor in determining the quality of the beams produced.

We have developed a technique to optimize the gun geometries using multi-objective genetic algorithms, which minimizes the beam emittance possible out of the gun while subject to a number of realistic constraints limiting the maximum fields in the gun. We outline our method, provide details on the parameterized gun geometries used in the study, and present the results of computer optimizations for low emittance beams possible from a short beamline that uses DC and (S)RF optimized gun geometries followed by an emittance compensation solenoid and a $\sim$ 1m drift.

METHOD DESCRIPTION

Parallel genetic algorithm

We have used a multiobjective evolutionary algorithm run on 160 2 GHz parallel processors to extensively survey the multivariate space for optimum solutions [2]. A detailed list of variable parameters (also known as decision variables) is given in Table 1. Refer to [2] and references therein for the description of inner workings of these algorithms. A brief summary follows for the convenience of the unfamiliar reader. The algorithm begins by running a trial set of solutions. Then the "fittest" solutions are selected from the set based on typically two criteria: beam emittance and the gun voltage or gradient. The optimizer seeks to minimize both objective parameters to produce a high brightness beam using a lower voltage in the gun (i.e. finds the smallest emittance possible at any given gun voltage). To form a new trial set for the next "generation", the algorithm applies two operators to the selected solutions of the previous generation: (1) "crossing" or "mating" of two or more solutions; and (2) slightly perturbing ("mutating") each solution to form new solutions ("offspring"). The process is then repeated with the new trial set and continues for a number of generations, effectively exploring the decision variable space for the best solutions. In the process, the solutions are subject to a set of constraints to ensure physically realistic scenarios. Finally, a set of optimal solutions is presented as the optimal front, the so-called "non-dominated set" or "Pareto front".

Treatment of field maps

Through parameterizations, the gun geometry is made a part of the decision variable space to be explored by

Table 1: Summary of parameters making up multivariate space.

Parameter Name	Comments
α_{DC}	DC gun angle
g_{DC}	DC gun gap
d_{DC}	DC gun recession
α_{SRF}	SRF gun angle
g_{SRF}	SRF gun gap
d_{SRF}	SRF gun recession
R_{SRF}	SRF gun photocathode curvature
E_{peak}	Peak E_z field strength in the gun
$SuperGaussian$	Super-gaussian nature of beam shape
Dip	Dip character of beam shape
$Ellipse$	Ellipse character of beam shape
$Slope$	Slope character of beam shape
$Tail$	Length of beam tail
$\sigma_{x,y}$	Laser spot size
B_{Peak}	Peak B_z field strength of the solenoid
$\sigma_{t,initial}$	Laser duration (fixed for DC guns)
ϕ_0	Initial RF phase (SRF gun only)

the multiobjective evolutionary algorithm. A space-charge code [3, 4] is then used to evaluate beam parameters for a given set of variable parameters (also known as decision variables) using realistic field maps obtained from E&M simulations. The electrostatic fields were obtained using POISSON for DC guns and SUPERFISH for SRF guns [5]. The fields are solved for prior to the optimization algorithm being run rather than being recalculated as a part of the optimization process. The possible gun geometries under exploration are indexed, and the optimizer uses these indexes to select the actual field map. This approach allows one to decouple the optimizer from a particular field map generating code making the optimizer applicable to a diverse set of problems. This is achieved, however, at the expense of requiring a larger amount of storage space, and that the geometry parameters are made available to the optimizer as part of a discrete, rather than continuous, range of values. Because of axial symmetry of the gun, the off-axis field expansion is employed, allowing compact representation of the field maps. E.g. with a typical 100GB storage, on the order of 10^6 field maps can be stored allowing sufficiently fine sampling of say 4-5 geometry parameters. Special care has been taken controlling the mesh quality and residual error in the field solver to ensure that the tabulated values of the field along the axis $E_z(z)$ can be correctly numerically differentiated twice to obtain the first non-linear term in the off-axis expansion.

OPTIMIZATION STUDY

Beamline

To study the effect of gun geometries, we have chosen a simple short beamline, which consists of the gun, the emittance compensating solenoid and a drift. Refer to Table 2.

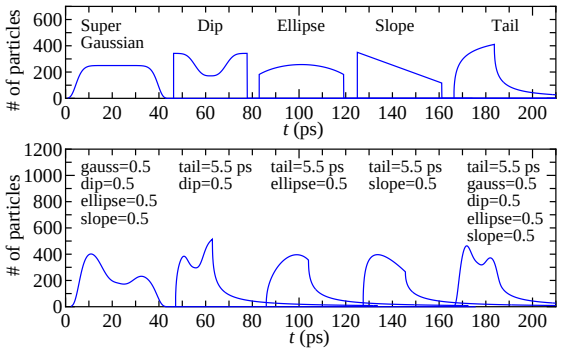

Figure 1: Illustration of the variable parameters specifying temporal laser profile. The top row shows the results of each of the parameters isolated. The second row shows examples of various combinations of parameters. The transverse profile is specified by the first three parameters (Super-gaussian, Dip, and Ellipse).

Laser shaping

The laser beam profile is specified by a set of variables [2] for each plane (transverse and longitudinal) varied over the interval [0-1] along with a tail parameter, as illustrated in Figure 1. Note, however, the temporal tail feature is not used in this study corresponding to the fact of GaAs being a prompt emitter when illuminated with the wavelength 520 nm [6, 7].

DC GUN STUDY

Parameterized gun geometry

The DC gun geometry is parameterized by the angle α_{DC} complementary to that of the electrode surfaces to the beamline, the z-displacement or gap g_{DC} between the electrodes, and the recession or deepening d_{DC} of the photocathode (Figure 2).

Voltage breakdown condition

In order to simulate realistic gun field strengths, empirical gun breakdown laws are enforced as constraints in the optimizations. Following [8], the data on high voltage breakdown from a wide set of measurements for large area electrodes is plotted in Figure 3 as a function of gap. The maximum field values allowed on the cathode electrode surface in the simulations (generally substantially larger than the cathode accelerating gradient, $E_{z,cath}$) are shown in Figure 4 as a function of the breakdown voltage.

Results

As mentioned earlier, increasing α_{DC} in the DC gun increases transverse focusing, but decreases longitudinal field strength at the cathode. Increasing the cathode-anode gap g_{DC} allows a larger voltage if operating near the breakdown, while it also reduces the available gradient at the

Table 2: Parameters and values associated with DC and SRF gun versions of the beamline used in simulations.

Parameter	Value in DC Gun Beamline	Value in SRF Gun Beamline
Gun photocathode location, z_{cath}	0	0
Solenoid location, z_{sol}	0.201 m	0.400 m
Emittance minimization point, z_ε	1.301 m	1.301 m
Thermal energy of photoelectrons, $k_B T_\perp$	120 meV	120 meV
Bunch charge, Q_{bunch}	80 pC	80 pC
Bunch length, $\sigma_{t,initial}$	12 ps	variable, 0-20 ps
Bunch shape	variable, see Fig. 1	variable, see Fig. 1

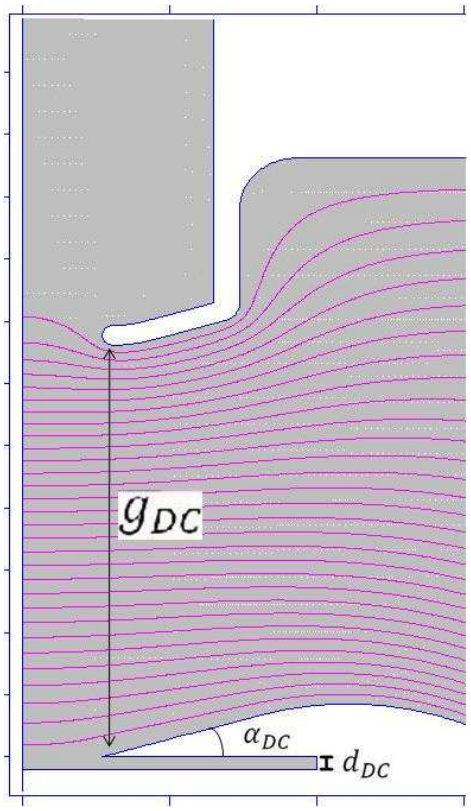

Figure 2: Closeup of the DC gun geometry, shown in the z-r plane, with the definitions of geometry parameters α_{DC}, g_{DC}, and d_{DC} illustrated. The vertical axis is the beamline z; the horizontal axis is that of the cylindrical coordinate r. Equipotential lines are shown.

photocathode and the transverse focusing kick. In addition, larger g_{DC} slightly diminishes the accelerating field at the cathode and the strength of the focusing kick.

The optimization process of choosing the optimal α_{DC} and g_{DC} results in geometries having an approximately 20° to 30° angle and a 32 mm to 42 mm gap, as can be seen in Figures 5 and 6. The photocathode field corresponding to these figures varies between 3.3 and 5 MV/m (the actual maximum field at the cathode electrode surface is substantially larger, see Fig. 4). It is a surprising result that the photocathode field is not chosen to be at the voltage breakdown limit for the lower gun voltages in the plot. This likely indicates that a particular transverse focusing at the

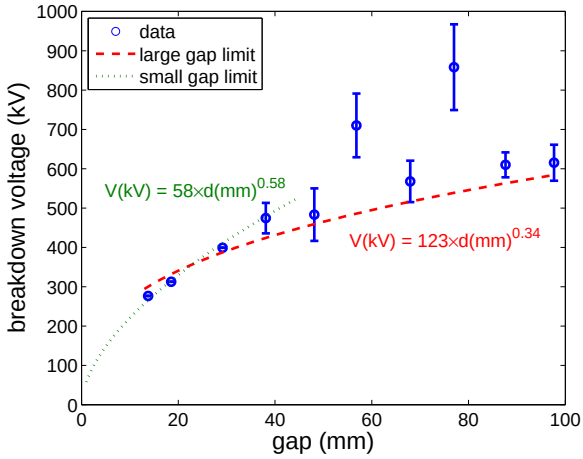

Figure 3: Adapted after [8]. Experimental data overlaid on the graph of breakdown voltage as a function of gap.

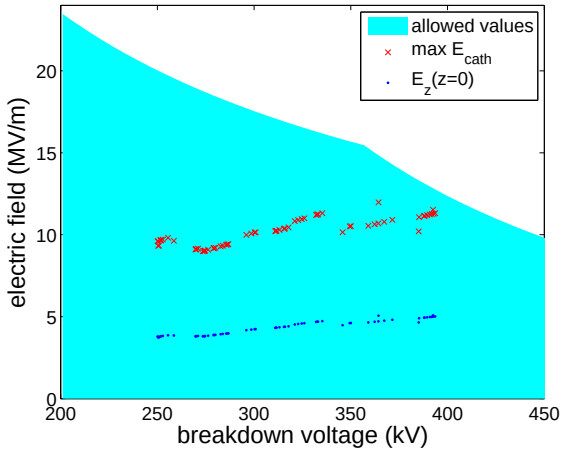

Figure 4: Simulation data from the DC gun optimization overlaid on the graph of maximum electric field as a function of breakdown voltage. $\max E_{cath}$ is the maximum electric field at the cathode electrode allowed under the breakdown constraint. $E_z(z = 0)$ is the electric field at the cathode chosen by the optimizer.

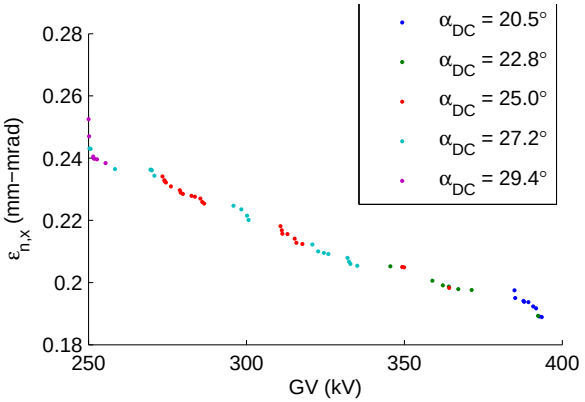

Figure 5: The resulting optimal front from the DC gun optimization after 254 generations, with each solution colored by its respective α_{DC}. The electron beam is represented with 28,000 macroparticles.

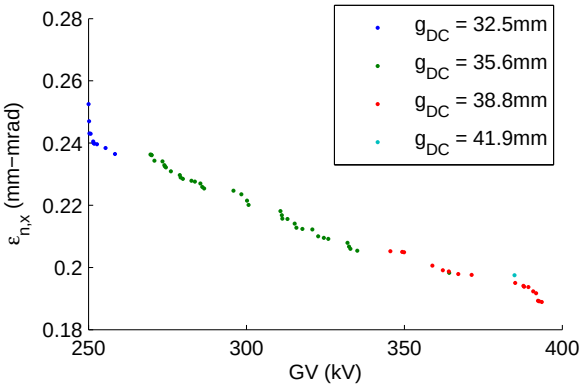

Figure 6: Optimal front from Figure 5, with each solution colored by its respective g_{DC}.

photocathode is crucial to achieving a high degree of emittance compensation. In addition, a shorter cathode-anode gap leads to a stronger unfavorable defocusing by the anode, which can be estimated using

$$\frac{1}{f_{anode}} \approx -\frac{1}{4g_{DC}} \frac{1 + eV_{gun}/mc^2}{1 + \frac{1}{2}eV_{gun}/mc^2}$$

with f_{anode} being the focusing length, eV_{gun} the kinetic energy after the gun, and mc^2 the electron rest mass energy.

The effect of photocathode recess for DC guns is discussed along with that for SRF guns in the next section.

SRF GUN STUDY

Parameterized gun geometry

For the optimization study, we have chosen a half-cell geometry. Additionally, we have simplified the SRF gun geometry from elliptically shaped, as required to mitigate multipacting, to a simpler shape shown in Figure 7 akin to a pillbox cavity. The SRF gun geometry is parameterized

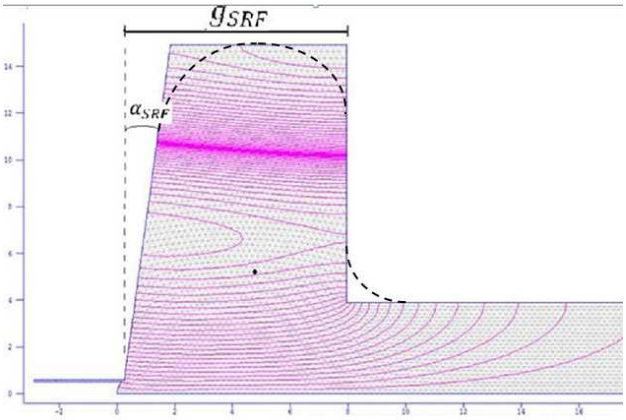

Figure 7: Simplified SRF gun geometry, shown in the z-r plane, with the definitions of the parameters α_{SRF} and g_{SRF} illustrated. The axes here are reversed from those used for the DC gun in Figures 2: the horizontal axis is the beamline z; the vertical axis is that of the cylindrical coordinate r. Lines of constant rH_ϕ, where H_ϕ is the magnitude of the azimuthal component of the magnetic field are shown.

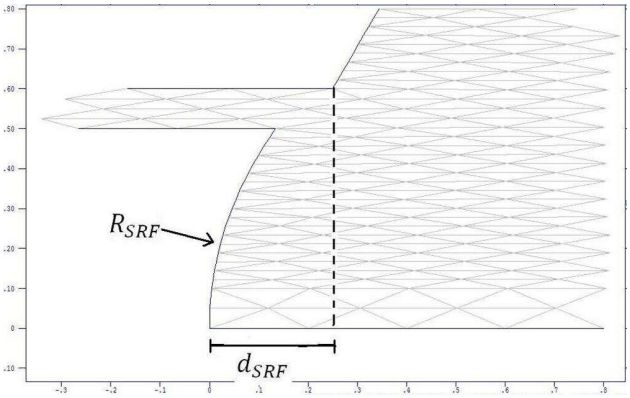

Figure 8: Close-up of the photocathode from Figure 7 with the definitions of the parameters d_{SRF} and R_{SRF} illustrated.

by the angle α_{SRF} complementary to that of the cathode surface to the beamline, the z-displacement or gap g_{SRF} between the photocathode and the other wall of the cavity, the deepening d_{SRF} and radius of curvature R_{SRF} of the photocathode surface (Figure 8), features originating from [9].

In the case of the SRF gun, an additional fourth parameter needs to be introduced to tune the cavity resonant frequency to 1.3 GHz, making it a dependent parameter. This fourth parameter is the equator radius of the cavity.

Cavity quenching condition

For a properly designed SRF gun, the field strength would be typically limited by the maximum achievable surface magnetic field $H_{SRF,crit}$ [10]. The routinely achieved surface fields in SRF cavities (TESLA 9-cell cavities oper-

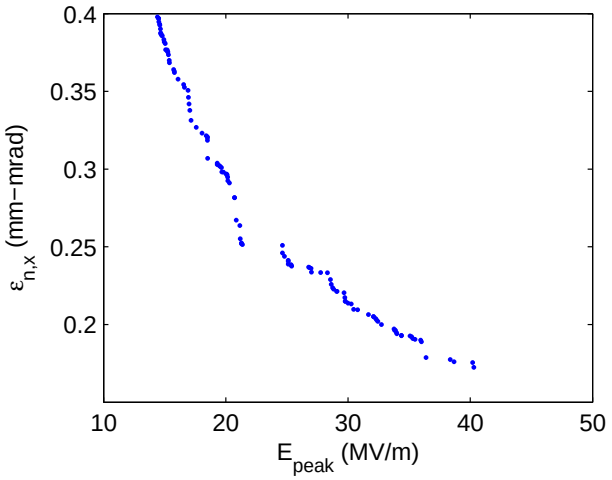

Figure 9: The resulting optimal front from the SRF gun optimization after ∼100 generations. The electron beam is represented with 28,000 macroparticles.

ating at 20 MV/m accelerating gradient) are slightly above $B_{SRF,crit} = 0.12\,\mathrm{T}$ [11]. Therefore, the SRF guns in this study have been chosen not to exceed $B_{SRF,crit} = 0.12\,\mathrm{T}$ to account for possible reduction in the gradient due to the introduction of the photocathode into the SRF gun cavity.

Results

Unlike α_{DC} in DC guns, increasing α_{SRF} in SRF guns was found to decrease focusing fields. Similar to DC guns, a larger α_{SRF} results in weaker longitudinal fields and limits the maximum achievable accelerating field by increasing the ratio of peak surface magnetic field to maximum accelerating gradient H_{pk}/E_{peak}. Therefore, a smaller α_{SRF} appears to be clearly favorable. Enlarging g_{SRF} was found to reduce the focusing fields in addition to slightly weakening the gradient at the photocathode.

The results of the SRF gun optimization are presented in Figure 9. The resulting optimum angle and gap for an SRF gun found through evolution are 7° to 12° and 30 mm to 41 mm respectively. The actual accelerating field at the photocathode at the moment of photoelectron emission varies from 4 to 17 MV/m in Figure 9. Note that our choice of the opening pipe (38 mm radius) may have effectively precluded the exploration of smaller g_{SRF} as the accelerating field tends to be dominated by the longer tail of $E_z(z)$ determined by the pipe opening. Smaller pipe openings will be investigated in [13].

The parameters d_{DC} and d_{SRF} are found to be "sloppy" [12] in the sense that they have a hardly noticeable effect on emittance (less than 5%, compared to keeping $d_{DC} = d_{SRF} = 0$).

Introducing curvature to the photocathode, on the other hand, boosts focusing fields right at the photocathode without sacrificing much the accelerating field. The optimization results support a curvature R_{SRF} of 15 mm.

CONCLUSION

We have presented gun geometry optimizations for DC and SRF guns. We show that very low emittance can be obtained from DC guns with moderate voltages sufficiently below the empirical voltage breakdown condition. SRF guns demonstrate a similar performance, although at larger peak electric fields, while not exceeding limits on the maximum achievable surface magnetic field. We investigate further the factors in the gun geometry affecting the beam brightness in [13].

REFERENCES

[1] I.V. Bazarov and G.A. Krafft, in USPAS course on Recirculated and Energy Recovered Linacs (2008), http://www.lepp.cornell.edu/∼ib38/uspas08/lec3.pdf.

[2] I.V. Bazarov and C.K. Sinclair, Physical Review Special Topics-Accelerators and Beams 8, 34202 (2005).

[3] K. Flottmann, http://www.desy.de/∼mpyflo/.

[4] S. van der Geer and M. de Loos, http://www.pulsar.nl/gpt.

[5] J. Billen and L. Young, Los Alamos National Laboratory, LA-UR-96-1834 (1996).

[6] I.V. Bazarov et al., Journal of Applied Physics, 103 (2008) 054901

[7] I.V. Bazarov et al., Physical Review Special Topics: Accelerator Beam 11 (2008) 040702

[8] P. Slade. The Vacuum Interrupter: Theory, Design, and Application. (CRC Press, 2007).

[9] D. Janssen and V. Volkov, Nuclear Inst. and Methods in Physics Research, A 452, 34 (2000).

[10] H. Padamsee, J. Knobloch, and T. Hays, RF superconductivity for accelerators (Wiley, 1998).

[11] V. Shemelin (2009), private communication.

[12] R. Gutenkunst, J. Waterfall, F. Casey, K. Brown, C. Myers, and J. Sethna, PLoS Comput Biol 3, e189 (2007).

[13] "Geometry optimization of DC and SRF guns to maximize beam brightness", in preparation